TRƯỜNG ĐẠI HỌC SÀI GÒN
TẠP CHÍ KHOA HỌC
ĐẠI HỌC SÀI GÒN
ISSN 1859 - 3208
Số 87, Tập 1, 2023

SAIGON UNIVERSITY
SCIENTIFIC JOURNAL
OF SAIGON UNIVERSITY
No. 87, Vol. 1, 2023

Email: tcdhsg@sgu.edu.vn ; Website: http://sj.sgu.edu.vn/

CRYSTAL STRUCTURE AND GAS-SENSING PROPERTIES OF THE HIERARCHICAL NANO/MICROSIZED α-Fe_2O_3 OXIDE PARTICLES SYNTHESIZED BY THE MODIFIED POLYOL PROCESS WITH HEAT TREATMENT

Tổng hợp, cấu trúc tinh thể, và các tính chất của các hạt nano/micro oxit α-Fe_2O_3 phân cấp bằng quy trình polyol có xử lý nhiệt

Nguyễn Việt Long[(1)(*)], Nguyễn Thị Nhật Hằng[(2)],
Lê Hồng Phúc[(3)], Nguyễn Hữu Trí[(1)], Hồ Văn Cừu[(1)]

[(1)]Trường Đại học Sài Gòn
[(2)]Trường Đại học Thủ Dầu Một
[(3)]Viện Hàn lâm Khoa học và Công nghệ Việt Nam

ABSTRACT

We have presented the synthesis of hierarchical α-Fe_2O_3 particles by a modified polyol method and heat treatment in air. The hierarchical α-Fe2O3 particles with the stable grains and the grain boundaries were characterized by XRD and SEM, and the gas sensing properties was analyzed by flow-through technique. Here, α-Fe_2O_3 particles at various hierarchical levels exhibited p-type behavior. A sensor device with the prepared material exhibiting the high quality of durability, response, and selectivity detected the existence of H_2, CO, and NH_3 gases. Finally, hierarchical α-Fe_2O_3 particles with the high stability of gas-sensing properties can be potentially used as promising candidates for gas-sensing sensor devices.

Keywords*: polyol process, heat treatment, Fe oxide, grain and grain boundary, sensor devices.*

TÓM TẮT

Chúng tôi trình bày kết quả nghiên cứu về tổng hợp các hạt α-Fe_2O_3 phân cấp bằng phương pháp polyol cải tiến và xử lý nhiệt trong không khí các hạt đó. Các hạt α-Fe_2O_3 thu được có cấu trúc phân cấp với các hạt ổn định, cấu trúc hạt và biên hạt được đặc trưng bởi các phép đo thực nghiệm XRD, SEM và cảm biến khí (sensor khí). Ở đây, các hạt α-Fe_2O_3 ở các cấp độ phân cấp khác nhau thể tính chất hoạt động của bán dẫn loại p. Một linh kiện cảm biến sử dụng vật liệu α-Fe_2O_3 đã được chế tạo có chất lượng cao về độ bền, đáp ứng và độ chọn lọc chất khí phát hiện được sự tồn tại của các khí H_2, CO và NH_3. Cuối cùng, các hạt α-Fe_2O_3 phân cấp có đặc tính nhạy khí có độ ổn định cao có thể được sử dụng làm loại vật liệu đại diện đầy triển vọng cho các thiết bị cảm biến khí.

Từ khoá: *qui trình polyol, qui trình xử lý nhiệt, oxit sắt, hạt và biên hạt, linh kiện cảm biến.*

[(*)]Corresponding author: nguyenvietlong@sgu.edu.vn

1. Introduction

The increasing presence of noxious gases derived from human activity, such as volatile organic compounds (VOCs), CO, SO_2, H_2S, NH_3, and NO_2, is the main cause of the increasingly serious air pollution. In particular, CO is one of the most dangerous gases to plants, animals, and humans. Therefore, the various gas sensor devices were designed for detection, diagnosis, and monitoring of toxic gases everywhere in public large cities and places [1-3]. Based on the huge demand for commercial oxide products, the scientists have been developing various gas-sensing oxide materials. The most common micro/nanomaterials are being used for this purpose, comprising ZnO, SnO_2, NiO, CuO, and carbon nanomaterials etc. [4-6].

To design cost-effective sensors, Fe oxides become promising candidates due to fast response, high sensitivity, and selectivity [4]. Among the oxide materials, Fe oxide micro/nanomaterials were developed for detection of air pollution from toxic CO gas as a specific gaseous species. Most of iron oxide nanoparticles were used in the nanosized ranges less than 100 nm according to various synthesis processes.

In our contribution, we present the controlled synthesis of hierarchical α-Fe_2O_3 particles by polyol methods with $NaBH_4$, NaOH, and heat treatment. α-Fe_2O_3 particles possess large sizes in the nano/microsized range. Each oxide particle shows the structure of smaller grains. Sensor device with hierarchical α-Fe_2O_3 particles was effectively used for the detection of carbon monoxide (CO), hydrogen (H_2), and ammonia (NH_3) in comparison with commercial Fe oxide nanoparticles in the nanosized range.

Our results of gas-sensing properties of the samples were presented in comparison with one sample (α-Fe_2O_3 particles with grain and grain boundary, and another commercial product α-Fe_2O_3 particles with a size range of 20-40 nm). The final formation of hierarchical α-Fe_2O_3 particles with grain and boundary nano/microsized structures led to a change from n-type to p-type semiconductor.

2. Materials and methods

Synthesis of hierarchical α-Fe_2O_3 particles by polyol method with PVP, $FeCl_3$ (and/or $FeCl_2$) $NaBH_4$, NaOH, and heat treatment at 900 °C was presented [6]. A polyol mediated synthesis was used for obtaining the as-prepared hierarchical α-Fe_2O_3 particles.

The various α-Fe_2O_3 particle powder samples were prepared for X-ray diffraction (XRD), and scanning electron microscopy (SEM). The crystal structure was found from the XRD pattern of α-Fe_2O_3 particles by Rigaku-D/max 2550V (40kV/200mA, CuKα1 at 1.54056Å). The most typical features of size, shape, and morphology of hierarchical α-Fe_2O_3 particles were investigated by field emission (FE)SEM.

For gas sensor fabrication, Fe oxide powders were homogeneously dispersed in dimethylformamide solution, and then coated onto a pair of comb-type Pt electrode deposited on thermally oxidized silicon substrate.

The gas-sensing characteristics of sensor device using hierarchical α-Fe_2O_3 particles were carefully measured by flow-through technique via standard flow rate of 400 sccm for both dry air and balanced gas in homemade sensing system. Gas-sensing characteristics were tested to H_2, CO, and NH_3 in a temperature range of 250-450°C.

Here, sensor response S was clearly defined as $S = R_{air}/R_{gas}$ for reducing gases, where Rgas and Rair are sensor resistance in the presence of testing gas and dry air, respectively.

The gas-sensing properties of two samples, commercial Fe_2O_3 particles (Fe_2O_3, 20-40 nm, Wako), and our as-prepared α-Fe_2O_3 particles with grain and grain boundary in present research will be compared in here.

3. Results and Discussion

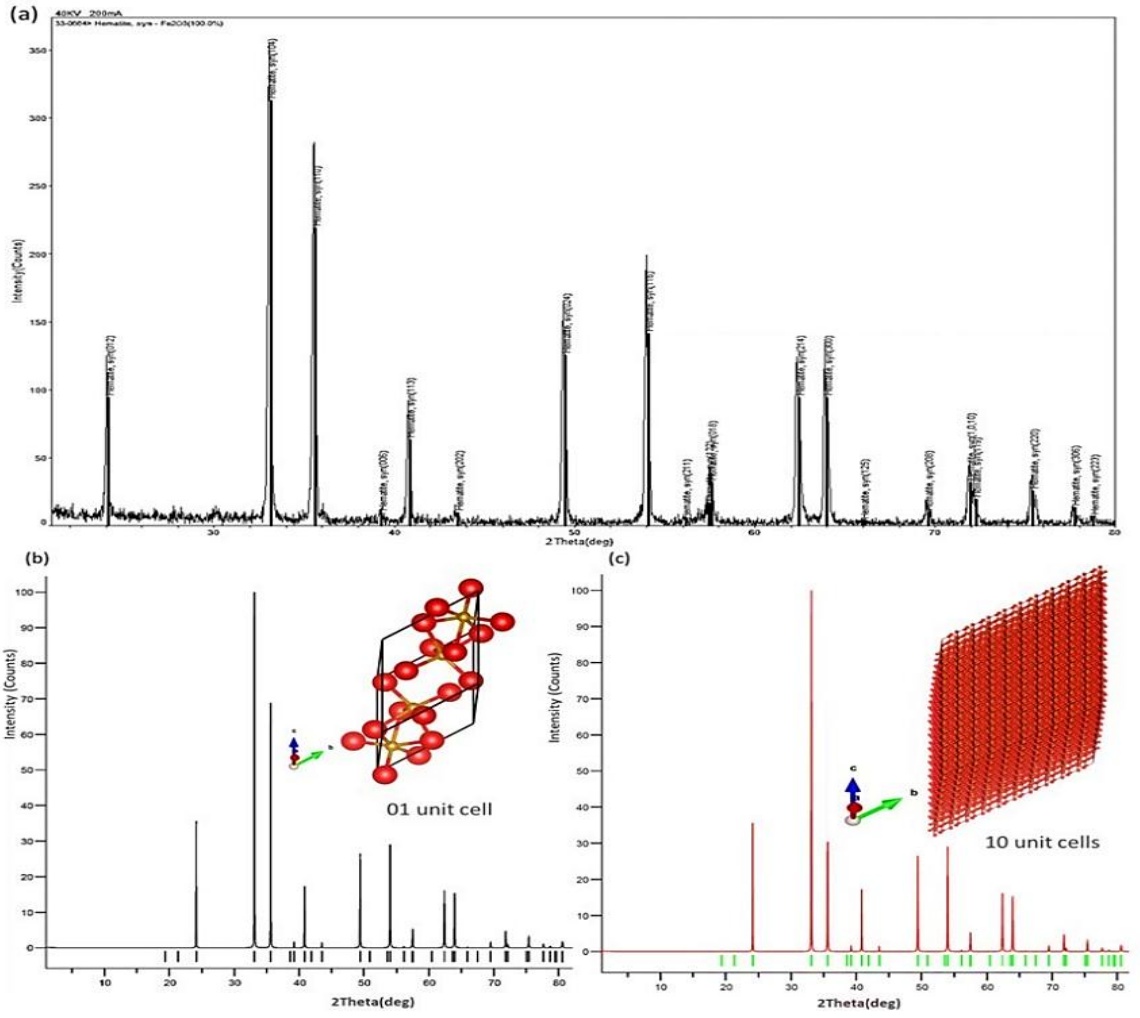


Figure 1. (a)-(c) Experimental XRD pattern of α-Fe_2O_3 particles, structure and crystallographic one unit cell and unit cells of α-Fe_2O_3 by Jade 6.0 version and Vesta software. Copyright 2006-2017 (K. Momma and F. Izumi) [25,31].

Figure 1(a) clearly shows the result and analysis of XRD of the as-prepared α-Fe_2O_3 particles with particle size of ~10 μm according to ICDD/JCPDS-PDF#33-0664 by Jade 6.0 version, and unit cells of α-Fe2O3, which demonstrates the typical and strong peaks at (012), (104), (110), (113), (024), (116), (122) or (018), (214), (300), (208), (1010), and (220), respectively in a 2θ range of 20-80°.

In fact, Figure 1(b) and (c) show that theoretical data and calculation of XRD of one-unit cell and ten-unit cells are relatively similar to the experimental XRD data and analysis.

Table 1. PDF#33-0664; Hematite, syn; Fe_2O_3; Radiation (CuKα1); Hexagonal R-3c(167).

2-Theta	d(Å)	I(f)	(h k l)	Theta	1/(2d)	2pi/d
24.138	3.684	30	(0 1 2)	12.069	0.1357	1.7055
33.152	2.7	100	(1 0 4)	16.576	0.1852	2.3271
35.611	2.519	70	(1 1 0)	17.806	0.1985	2.4943
40.854	2.207	20	(1 1 3)	20.427	0.2266	2.8469
49.479	1.8406	40	(0 2 4)	24.74	0.2717	3.4137
54.089	1.6941	45	(1 1 6)	27.045	0.2951	3.7089
57.428	1.6033	5	(1 2 2)	28.714	0.3119	3.9189
57.589	1.5992	10	(0 1 8)	28.794	0.3127	3.929
62.449	1.4859	30	(2 1 4)	31.225	0.3365	4.2285
63.989	1.4538	30	(3 0 0)	31.995	0.3439	4.3219
69.599	1.3497	3	(2 0 8)	34.799	0.3705	4.6552
71.935	1.3115	10	(1 0 10)	35.968	0.3812	4.7908
75.428	1.2592	8	(2 2 0)	37.714	0.3971	4.9898
77.727	1.2276	4	(3 0 6)	38.864	0.4073	5.1183
78.758	1.2141	2	(2 2 3)	39.379	0.4118	5.1752

As shown in Figure 1, the XRD data indicates that α-Fe_2O_3 crystal phase was formed with high crystallization, [7] corresponding to the strongest line (104) at 2θ degree of around 31.52°, and the corresponding eight strong lines experimentally found out in its good crystal phases and crystal parameters, i.e., 2Theta, d(Å), 1/2d, I(f), (hkl), Theta, 2π/d, respectively (Table 1).

Figure 2 illustrates SEM images of one sample of α-Fe_2O_3 particles with a size range of 10 μm with grain and grain boundary after heat treatment at 900°C h in air for 1 h. It is clearly observed that α-Fe_2O_3 particles show different rod-, arrow-, star-, spherical-type, and polyhedral shapes with micro/nanotextures, and with the deformations of size, shape, and morphology as well as their self-assembly and combination of the prepared particles. Herein, the powder product of α-Fe_2O_3 particles was regarded as hierarchically hexagonal micro/nanostructured crystal particles.

The as-prepared α-Fe_2O_3 particles with the grain and grain boundary were shown in Figure 2(a-d)) with the typical various kinds of the sizes of the grains and grain boundaries.

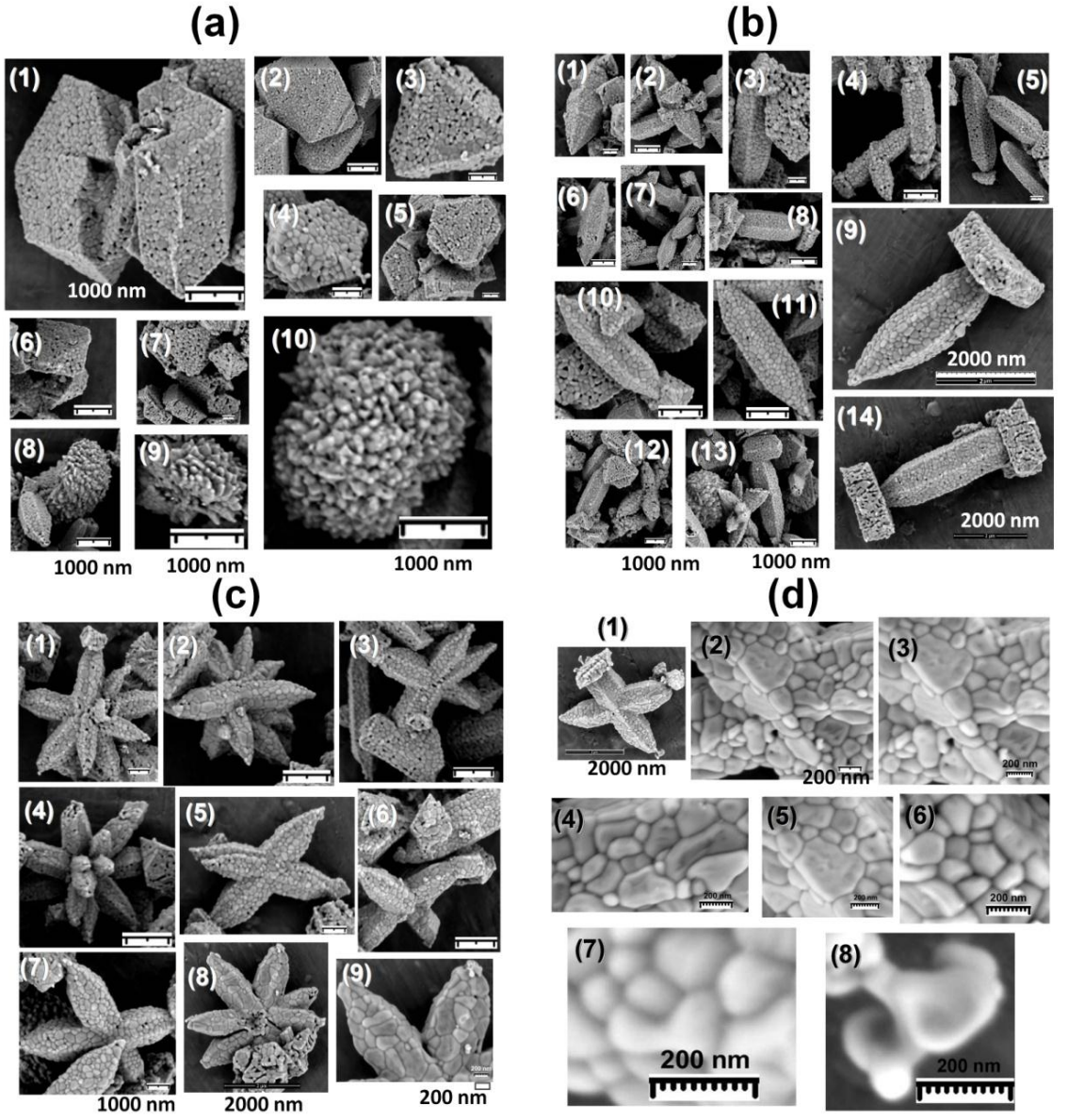


Figure 2. (a): (1-10) SEM images of α-Fe_2O_3 particles. (8-10) Spherical types. (b): (1-14) Rod types. (c): (1-9) Star types. (d): (1) Star type. (2-8) Oxide nano/microstructures with grain and grain boundary.

Recently, various fabrication methods have been successfully employed for preparing iron oxide materials, particularly modified polyol methods with heat treatment with various sizes and shapes. [8-17].

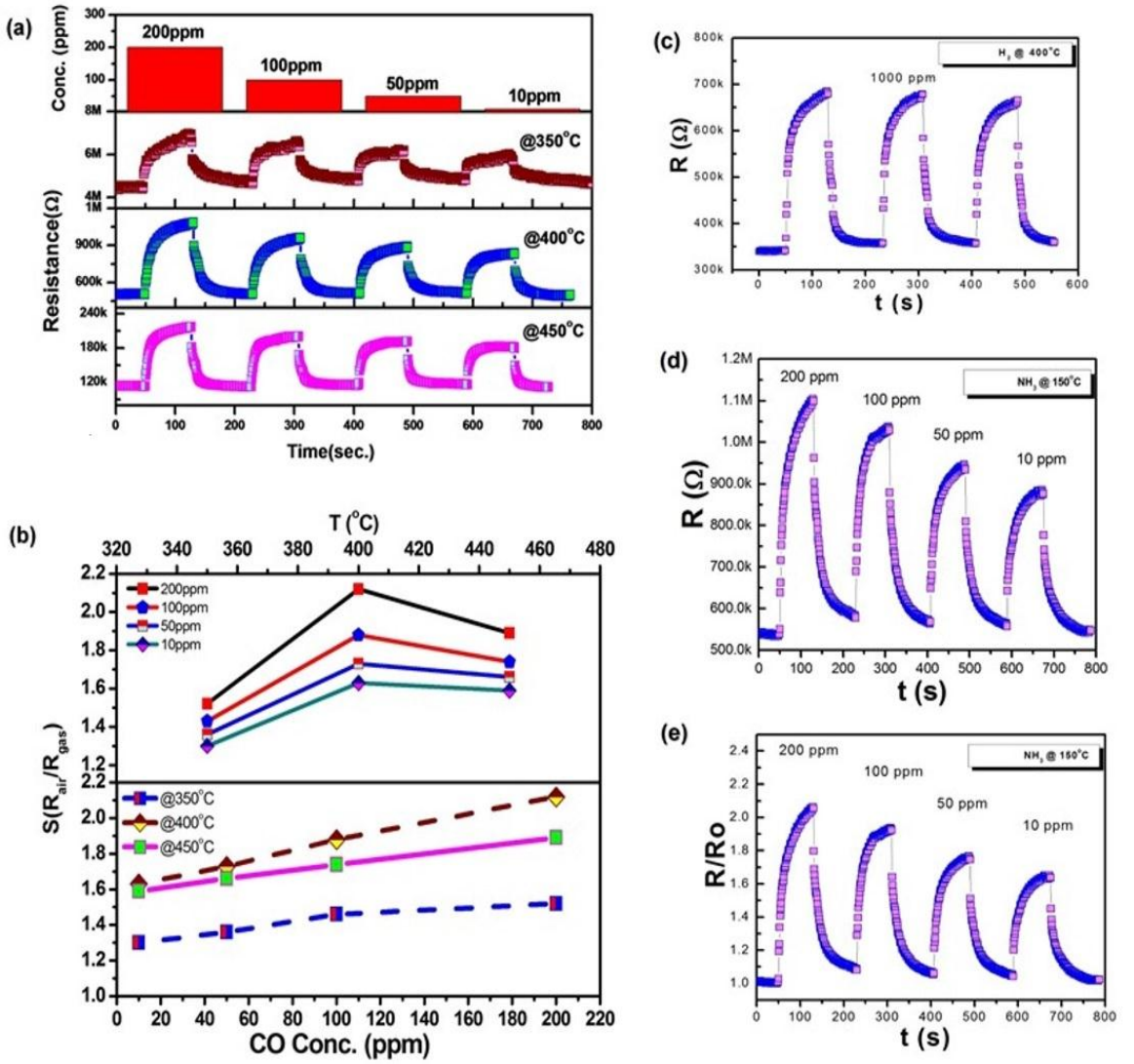


Figure 3. (a) Gas-sensing properties of Fe oxide nanoparticles at nanoscale (2-40 nm) as standard sample from Wako company (or using from Sigma-Aldrich). (b)-(e). Gas-sensing properties of hierarchical α-Fe_2O_3 particles to CO, H_2 and NH_3, respectively.

In a survey of CO gas-sensing properties, a standard sample of commercial α-Fe_2O_3 nanoparticles in the size range of 20-40 nm from Wako company was studied through the measurement of resistor changes according to the different concentrations of gases in a temperature range from 250 to 450 °C. In Figure 3a, at the different measured temperature points, R values of gas-sensing devices were significantly increased with the different concentrations at 200, 100, 50, and 10 ppm, respectively. This phenomenon demonstrated that the as-synthesized material was p-type semiconductor, of which the major type of charge carriers is determined to be holes. The literature study pointed out that α-Fe_2O_3 was an n- or p-type semiconductor depending on the stoichiometric of raw materials [18]. The

typical n-type semiconducting property of α-Fe_2O_3 was ascribed due to the presence of oxygen vacancy, while the typical p-type behavior caused by oxygen excessiveness in the crystal [19]. Herein, our samples were isothermally annealed at 900 °C, which led to the excessiveness of oxygen in the stoichiometry of materials, thus showing p-type behavior. When measured in atmosphere, oxygen molecules were adsorbed on the surface of the prepared material, of which oxygen exists mostly as ions like O^{2-}, O^-, and O^{2-} that received electron to form a zone of charge accumulation [20-22]. When sensor device measured the flow of CO reducing gases, CO molecules reacted and exchanged with oxygen ions adsorbed on the surfaces and returned electrons to the material. These electrons then combined with free holes that known as basic carriers in p-type material, thus reducing the main carrier concentration. This leads to an increase of resistance of sensor device [20-22]. Both response and recovery times of the material used were improved at the working temperature ranged from 250 to 450 °C (Figure 3). Here, response and recovery times were calculated at 200 ppm at different temperatures of 250, 300, 350, 400, and 450 °C. Accordingly, the obtained correspondent values were15s/30s, 10s/20s, 7s/15s, 5s/10s, and 3s/7s, respectively. Figure 3b shows a change in temperature response when measured with different gas concentrations. At about 400 °C, gas sensor represented the highest response levels amongst various gas concentrations. The response dependence as a function of CO concentration was measured at different temperatures, as presented in Figure 3c. Gas response increased linearly with gas concentrations over all measured temperature range. Gas responses at 400 °C show the highest levels, and reach the values of 1.6, 1.71, 1.88, and 2.11, corresponding to gas concentrations of 10, 50, 100, and 200 ppm, respectively. H_2 gas-sensing property of sensor device was studied at 400 °C in Figures 3d and e. Similar to CO gas, response to H_2 was measured by 1000 ppm (H_2), and the resistance of sensor device was increased twofold. H_2 gas response of sensor device for three cycles shows the similar gas-sensing property.

This confirms that the fabricated material was highly durable. Response and recovery times were 40s and 15s, respectively. Although sensor device responded to H_2 gas, the value of this response was much lower than that of CO. If we took response rate divided by gas concentration, response rate of H_2 and CO was 2/1000 and 2.11/200. Thus, sensor device consisting of α-Fe_2O_3 particles shows the better sensitivity toward CO gas compared to that of H_2 gas. In Figure 3d, we have also studied the sensitivity of sensor device with NH_3 at 150 °C.

Additionally, sensor device responded to NH_3 gas concentration in a range from 10 to 200 ppm at a temperature of 150 °C. The values of NH_3 gas response of sensor device at 10, 50, 100, and 200 ppm were 1.64, 1.76, 1.94, and 2.05, respectively. However, gas sensing response at a value to NH_3 was considered to be relatively equivalent to response value to CO gas.

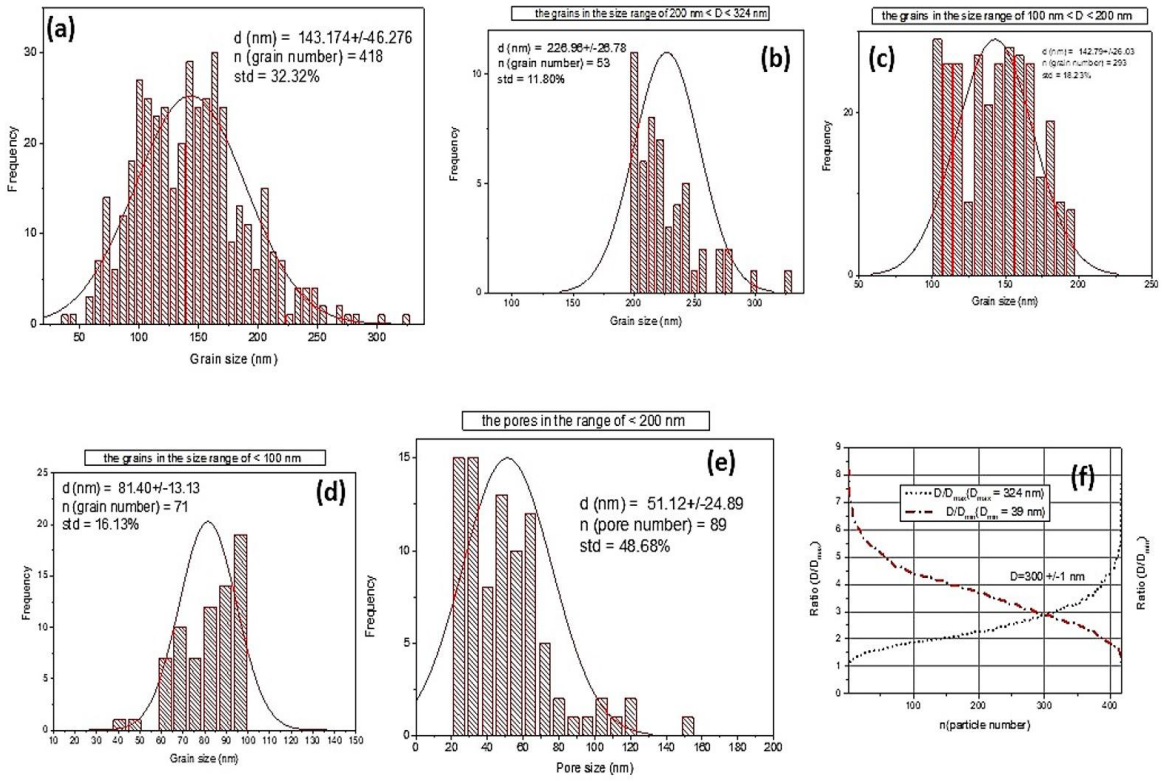


Figure 4. (a)-(e) The corresponding grain and pore size distribution histograms of the seen surface of hierarchical α-Fe_2O_3 particles. (f) The ratio of D/Dmax and D/Dmin: Dmax and Dmin are the estimated largest grain size and the estimated smallest grain size.

Figure 4 shows the distribution histograms of grain (Figure 4a-d), and pore size (Figure 4e) of one typical hierarchical α-Fe_2O_3 particle for the oxide grain size. The data of Figure 2 was based on the main size ranges, consisting of (i) the oxide grains less than 100 nm (for the fine oxide grains), (ii) the oxide grains calculated in the corresponding range of about 100 nm < D < 200 nm (for the intermediate oxide grains), and (iii) the oxide grains in the corresponding range of about 200 nm < D < 324 nm (for the large raw oxide grains). This shows that the average grain and pore sizes on the surface of one prepared particle with their different standard deviations are different. The smallest and largest sizes of oxide grain are determined to be approximately 39 nm and 324 nm, respectively. Furthermore, it can be clearly seen that the pore sizes of particles ranged from 26 nm to 150 nm. Recently, scientists have proved the irreplacable role of grain growth, grain size, and grain boundary as the frontliners in the formation of novel structures for use in theory and experiment, particularly in the field of magnetic materials and simulation. Figure 4f shows the ratio of grain size (D) to the largest grain size, and the smallest grain size. The observed results proved that with a ratio of 1.0, we are able to achieve a homogeneous grain system for the average size ranged from 324 nm (the large oxide grains) to 39

nm (the small oxide grains). The growth of the α-Fe_2O_3 oxide is very abnormal when the high ratio is higher than 8.0. When D values were in the range of 2.0-4.0, we probably possessed a relative homogeneous system with the grain size of about 300 nm as estimated. Recently, the researchers have pointed out the important role of grain growth, grain size, and grain boundary in the design of novel structures for applications in theory and experiment [23-25]. It is convinced that the hierarchical α-Fe_2O_3 oxide spheres, polyhedrons, rods are formed from nano to microscale. The as-prepared particles were arranged in a unique texture, of which a grain is connected by another grain boundary. Their new nano/microsized structures were formed by heat treatment process at the high temperature. Thus, the clear formation of the pores possibly led to an improvement of gas sensitivity of the nano/microscale oxide material. It is certain that α-Fe_2O_3 with grain and grain boundary as gas-sensing elements boundary indicated their high sensitivity. At present, it is known that controlling the grain and grain boundary structure of nano/microsized oxides with the nano/microsized pores is the challenge to researchers. The nano/microstructures oxide products used can be wet, dry, and heated, respectively [26-30]. According to this investigation, nano/microstructures oxide powders were used in the form of dried and heated powders. At present, the researchers show that α-Fe_2O_3 is one of the most important kinds of materials in gas-sensing materials roadmap [32].

4. Conclusions

In this contribution, we have used the α-Fe_2O_3 particles for detection and analysis of gases. In comparison, sensor device using α-Fe_2O_3 particles (1000-10000 nm) with large nano/microscale exhibited the good response of CO as high as commercial α-Fe_2O_3 nanoparticle product with narrow nanoscale (2-40nm) for gas sensor devices for the detection of CO, H_2, and NH_3 gases, respectively. SEM images show that nano/microsized particles were combined to form large clusters with different shapes that contributed to increasing the sensitivity of gas sensing. Thus, the critical issue of the size (nano/microscale ranges) can be well understood in the viewpoint of the as-prepared interesting nano/microsized structures.

Acknowledgments: Our research was supported by Saigon University through Grant number CSA2022-20.

REFERENCES

[1] H. J. Kim and J. H. Lee, (2014). "Highly sensitive and selective gas sensors using p-type oxide semiconductors: Overview." *Sens. Actuators. B. Chem.*, 192, pp. 607-627.

[2] D. R. Miller, S. A. Akbar, and P. A. Morris, (2014). "Nanoscale metal oxide-based heterojunctions for gas sensing: a review." *Sens. Actuators. B. Chem.*, 204, pp. 250-272.

[3] G. Eranna, B. C. Joshi, D. P. Runthala, and R. P. Gupta, (2014). "Oxide materials for development of integrated gas sensors - a comprehensive review." *Crit. Rev. Solid. State Mater. Sci.*, 29(3-4), pp. 111-188.

[4] A. Stanoiu, A. C. Kuncser, D. Ghica, O. G. Florea, S. Somacescu, and C. E. Simion, (2021). "Sensing Properties of NiO Loaded SnO_2 Nanoparticles-Specific Selectivity to H_2S." *Chemosensors*, 9(6), 125 (16 pages).

[5] E. Navarrete, C. Bittencourt, P. Umek, and E. Llobet, (2018). "AACVD and gas sensing properties of nickel oxide nanoparticle decorated tungsten oxide nanowires." *J. Mater. Chem. C*, 6(19), pp. 5181-5192.

[6] N. V. Long, T. Teranishi, Y. Yang, C. M. Thi, Y. Cao, and M. Nogami, (2015). "Iron oxide nanoparticles for next generation gas sensors." *Int. J. Metall. Mater. Eng.*, 1(1), pp. 1-18.

[7] W. Qin, C. Yang, R. Yi, and G. Gao, (2011). "Hydrothermal Synthesis and Characterization of Single-Crystalline [alpha]-Fe_2O_3 Nanocubes." *J. Nanomater.*, Article ID 159259, 5 pages.

[8] H. Dong, Y. C. Chen, and C. Feldmann, (2015). "Polyol synthesis of nanoparticles: status and options regarding metals, oxides, chalcogenides, and non-metal elements." *Green Chem.*, 17(8), pp. 4107-4132.

[9] N. V. Long, Y. Yang, C. M. Thi, Y. Cao, and M. Nogami, (2014). "Ultra-high stability and durability of α-Fe_2O_3 oxide micro-and nano-structures with discovery of new 3D structural formation of grain and boundary." *Colloids. Surf. A.*, 456, pp. 184-194.

[10] N. V. Long, Y. Yang, T. Teranishi, C. M. Thi, Y. Cao, M. Nogami, (2015). "Related magnetic properties of $CoFe_2O_4$ cobalt ferrite particles synthesised by the polyol method with $NaBH_4$ and heat treatment: new micro and nanoscale structures." *RSC Adv.*, 5(70), pp. 56560-56569.

[11] N. V. Long, Y. Yang, C. M. Thi, B. T. Hang, Y. Cao, and M. Nogami, (2015). "Controlled synthesis and characterization of iron oxide micro-particles for Fe-air battery electrode material." *Colloid. Polym. Sci.*, 293(1), pp. 49-63.

[12] N. V. Long, Y. Yang, C. M. Thi, N. V. Minh, Y. Cao, M. Nogami, (2013). "The development of mixture, alloy, and core-shell nanocatalysts with nanomaterial supports for energy conversion in low-temperature fuel cells." *Nano Energy*., 2(5), pp. 636-676.

[13] N. V. Long, Y. Yang, M. Yuasa, C. M. Thi, Y. Cao, T. Nann, M. Nogami, (2014). "Gas-sensing properties of p-type α-Fe_2O_3 polyhedral particles synthesized via a modified polyol method." *RSC Adv.*, 4(16), pp. 8250-8255.

[14] N. V. Long, Y. Yang, M. Yuasa, C. M. Thi, Y. Cao, T. Nann, M. Nogami, (2014). "Controlled synthesis and characterization of iron oxide nanostructures with potential applications for gas sensors and the environment." *RSC Adv.*, 4(13), pp. 6383-6390.

[15] N. V. Long, Y. Yang, T. Teranishi, C. M. Thi, Y. Cao, M. Nogami, (2015). "Synthesis and magnetism of hierarchical iron oxide particles." *Mater. Design.*, 86, pp. 797-808.

[16] N. V. Long, Y. Yang, C. M. Thi, M. Nogami, (2017). "Controlled Synthesis and Magnetic Properties of Uniform Hierarchical Polyhedral α-Fe_2O_3 Particles." *J. Electron. Mater.*, 46(6), pp. 3301–3308.

[17] N. V. Long, Y. Yang, C. M. Thi, and M. Nogami, (2017). "Controlled Synthesis and Ferrimagnetism of Homogeneous Hierarchical $CoFe_2O_4$ Particles." *J. Electron. Mater.*, 46(10), pp. 6001-6008.

[18] Y. C. Lee, Y. L. Chueh, C. H. Hsieh, M. T. Chang, L. J. Chou, Z. L. Wang, Y. W. Lan, C. D. Chen, H. Kurata, and S. Isoda, (2017). "p-Type α-Fe_2O_3 Nanowires and their n-Type Transition in a Reductive Ambient." *Small.*, 3(8), pp. 1356-1361.

[19] A. Serrano, J. López-Sánchez, I. Arnay, R. Cid, M. Vila, E. Salas-Cólera, G. R. Castro, and J. Rubio-Zuazo, (2021). "Improving the CO and CH_4 Gas Sensor Response at Room Temperature of α-Fe_2O_3 (0001) Epitaxial Thin Films Grown on $SrTiO_3$ (111) Incorporating Au (111) Islands." *Coatings*, 11, 848 (12 pages).

[20] G. Li, X. Wang, H. Ding, and T. Zhang, (2012). "A facile synthesis method for $Ni(OH)_2$ ultrathin nanosheets and their conversion to porous NiO nanosheets used for formaldehyde sensing." *RSC Adv.*, 2(33), pp. 13018-13023.

[21] H. Nguyen, and S. A. El-Safty, (2011). "Meso-and macroporous Co_3O_4 nanorods for effective VOC gas sensors." *J. Phys. Chem. C.*, 115(17), pp. 8466-8474.

[22] N. D. Hoa, and S. A. El-Safty, (2011). "Gas nanosensor design packages based on tungsten oxide: mesocages, hollow spheres, and nanowires." *Nanotechnol.*, 22(48), 485503.

[23] S. Hirosawa, M. Nishino, and S. Miyashita, (2017). "Perspectives for high-performance permanent magnets: applications, coercivity, and new materials." *Adv. Nat. Sci.: Nanosci. Nanotechnol.*, 8(1), 013002.

[24] N. V. Long, Y. Yang, C. M. Thi, V. P. Tuyen, and M. Nogami, (2018). "Hierarchical micro/nanoscale $NdFe_{11}Co$ oxide and alloy materials synthesized by polyol mediated methods with heat treatment." *Mater. Lett.*, 212, pp. 202-206.

[25] K. Momma and F. Izumi, (2011). "VESTA 3 for three-dimensional visualization of crystal, volumetric and morphology data." *J. Appl. Cryst.*, 44(6), pp. 1272-1276.

[26] Z. Lu and Y. Yin, (2012). "Colloidal nanoparticle clusters: functional materials by design." *Chem. Soc. Rev.*, 41(21), 6874-6887.

[27] J. Liu, Z. Sun, Y. Deng, Y. Zou, C. Li, X. Guo, L. Xiong, Y. Gao, F. Li, and D. Zhao, (2009). "Highly water-dispersible biocompatible magnetite particles with low cytotoxicity stabilized by citrate groups." *Angew. Chem. Int. Ed.*, 48(32), pp. 5875-5879.

[28] B. Peng, X. Zhang, D. G. Aarts, and R. P. Dullens, (2018). "Superparamagnetic nickel colloidal nanocrystal clusters with antibacterial activity and bacteria binding ability." *Nat. Nanotechnol.*, 13(6), pp. 478-482.

[29] N. V. Long, Y. Yang, C. M. Thi, M. Nogami, (2017). "Polyol-Mediated Synthesis, Microstructure and Magnetic Properties of Hierarchical Sphere, Rod, and Polyhedral α-Fe_2O_3 Oxide Particles." *J. Electron. Mater.*, 46(6), pp. 3615-3621.

[30] W. Wu, Z. Wu, T. Yu, C. Jiang, W. S. Kim, (2015). "Recent progress on magnetic iron oxide nanoparticles: synthesis, surface functional strategies and biomedical applications." *Sci. Technol. Adv. Mater.*, 16, 023501 (43 pages).

[31] http://www.crystallography.net/cod/9000139.html.

[32] H. Wang, *et al.*, (2021). "Gas Sensing Materials Roadmap." *J. Phys.: Condens. Matter.*, 33, 303001, pp. 1-72.

Ngày nhận bài: 14/11/2023 Ngày chấp nhận đăng: 14/12/2023